International Journal of Mechanical, Industrial and Aerospace Sciences
ISSN: 2517-9950
Vol:7, No:10, 2013

Investigation of Hydraulic and Thermal Performances of Fin Array at Different Shield Positions without By-Pass

Ramy H. Mohammed

***Abstract*—**In heat sinks, the flow within the core exhibits separation and hence does not lend itself to simple analytical boundary layer or duct flow analysis of the wall friction. In this paper, we present some findings from an experimental and numerical study aimed to obtain physical insight into the influence of the presence of the shield and its position on the hydraulic and thermal performance of square pin fin heat sink without top by-pass. The variations of the Nusselt number and friction factor are obtained under varied parameters, such as the Reynolds number and the shield position. The numerical code is validated by comparing the numerical results with the available experimental data. It is shown that, there is a good agreement between the temperature predictions based on the model and the experimental data. Results show that, as the presence of the shield, the heat transfer of fin array is enhanced and the flow resistance increased. The surface temperature distribution of the heat sink base is more uniform when the dimensionless shield position equals to 1/3 or 2/3. The comprehensive performance evaluation approach based on identical pumping power criteria is adopted and shows that the optimum shield position is at x/l=0.43.

***Keywords*—**Shield, Fin array, Performance evaluation, Heat transfer, Validation.

I. Introduction

THE constant demand for speed and performance in electronics is unfortunately accompanied by ever increasing thermal dissipation. Air heat exchangers or heat sinks continue to be the most viable thermal solution for the electronics industry primarily because of low cost and high reliability. Heat sinks for electronics depend on conduction from the electronic package to the heat sink base, followed by conduction into the extended surfaces and convection to the flow. Hence, arrangement, shape, and orientation of extended surfaces play the main role in the thermal dissipation. Many authors have undertaken the characterization of parallel plate heat exchangers. Among research published on heat sinks to improve the cooling of electronic components, Knight et al. [1] analytically characterized the flow and heat transfer behavior of such heat exchangers as function of geometry and fluid characteristics, for developing and fully developed flow.

Teertstra et al. [2] similarly found analytical solutions for such configurations, and blended both regimes into a single solution for a wide range of Reynolds number.

Lee [3] studied the effects of flow by-pass, by allowing flow around the heat exchanger in a partially confined flow configuration. Butterbaugh and Kang [4] treated this case by constructing a nodal network of flow paths, and detailed the calculation of each network element. They accounted not only for flow by-pass, but also for that part of the flow that enters the heat sink and exits through the top, the so-called tip leakage.

Similarly, Shaukatullah et al. [5] measured the thermal performance for in-line square pin fins and plate heat sinks for different fin thickness, spacing, height, and angle of approach for velocities under 5 m/s, while allowing flow to partially by-pass the exchanger. More recently, Jonsson and Moshfegh [6] experimentally characterized plate and circular, rectangular and strip pin fins, in both staggered and in-line configurations for different dimensions, allowing for variations on tip and side by-pass. Generally, most of the studies have not been especially useful for extracting local friction or heat transfer coefficients. Dogruoz et al. [7] investigated the hydraulic resistance and thermal performance of in-line square-pin fin heat sinks; their predictions based on a two-branch by pass model agreed satisfactorily with experimental data at large velocities of approach for tall heat sinks, but the discrepancy increased with decreasing approach velocity and height of the heat sink.

El-Sayed et al. [8] investigated the effects of the fin arrays geometries and also the fin tip-to-shroud clearance on the heat transfer, the fluid flow and the pressure drop characteristics of longitudinal rectangular-fin arrays. During the experiments, different geometrical parameters were varied such as the fin height, fin thickness, inter-fin space, fins number, and fin tip-to-shroud clearance were varied parametrically; starting with the no-clearance case.

CFD approaches have been extensively applied to study flow and heat transfer in heat sinks, for example by Jonsson and Moshfegh [9], Biber and Belady [10], and Dvinsky et al. [11]. Dvinsky et al. [11] used CFD to study in detail flow and heat transfer behavior for in-line and staggered heat sinks for the approach velocities of 1, 3 and 5 m/s. Because their study allowed for both top and side flow by-pass, their results help to elucidate the deficiencies of a simple 2(or even 4) path model that does not allow for leakage from the heat sink, back to the channel. They found that, when allowing side and top clearance, up to half of the flow that enters the heat sink may leave it through the side and top. CFD simulations of Jonsson and Moshfegh [9] revealed that this leakage flow may be quite complex. They reported inward flow from the sides, to balance flow lost through the top. Li et al. [12] investigated

R. H. Mohammed is with the Zagazig University, CO 44519 Egypt, (phone: 201114049331; e-mail: Rhamdy@ Zu.edu.eg).

numerically the hydraulic and thermal performance of a plate fin heat sink with a shield. The decrease of thermal resistance due to the shield diminishes with increasing fin height, but increasing the width of the fins has a more radical effect. For a shield at a particular Reynolds number, the fin geometry should be selected carefully to fit the demands of enhanced effectiveness of heat transfer and decreased power consumption. Tsai et al. [13] investigated the effect of the inclination angle of a plate heat shield on thermal and hydraulic performance of a plate fin heat sink. It found that the minimum pressure drops for smaller fin heights appear for inclination angles of shield about 90° to 105°. The minimum pressure drops for the largest fin height are ambiguous. Zhang et al. [14] investigated experimentally the heat transfer performances of the fin array with shield in the bypass. Experimental results indicated that the heat transfer and flow performances of fin array were marginally influenced by the power input. Evaluated under the identical pressure drop and the identical pumping power criteria, the optimum position of shield was the position where the dimensionless shield position equaled 0, and the optimum shield height was half of the fin height. Finally, the correlations of mean Nusselt number and friction factor were fitted considering the influences of Reynolds number, the shield position and the shield height. The predicted values fitted the experimental data with the deviations less than ±15.0%.

As the previous literatures indicated, it was a feasible way to enhance the heat transfer of fin array by changing the bypass structure and shield inclination angle. The shield was an enhancement device for the fin array with/without bypass, and had a wide field of application with good prospects. The focus of the present work is to experimentally and numerically investigate the effect of a shield position on the hydraulic and thermal performance of pin fin heat sink. Comprehensive performance evaluation of fin array with different shield position is presented. Therefore, we try to find the optimum shield position where lowest thermal resistance is occurred.

II. Experimental Work

A. Experimental Apparatus and Measurements

The experimental apparatus consists of the main supply duct, test section, tested models as shown in Fig. 1. The main duct which supplies air to the test section contains air blower, air gate to adjust the mass flow rate of the air through the working section, a flow straighteners (screens) at the air inlet side of the wind tunnel, honeycombs to reduce the swirl motion of the air stream and to break up occasional large eddies that may reach the test section, and flow orifice to measure the air flow rate.

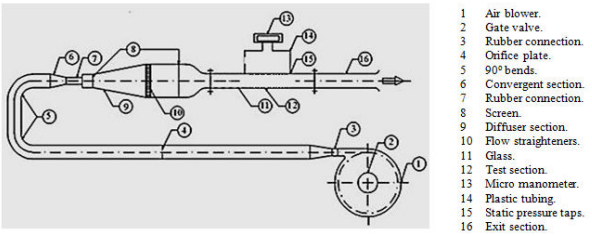

Fig. 1 Schematic diagram of test rig and instrumentation

The main supply duct runs from the blower discharge exit up to the inlet of the test channel. This duct consists of two parts: the first part is a U-shaped circular pipe of 75mm inner diameter and connected to blower exit via a conical diffuser. The other end of the U-shape is connected to the second part of the main supply duct via a conical nozzle. The second part of the supply duct that precedes the test channel is 1.0m long and consists of a diffuser, a settling length and a contraction. This part of the supply duct is fitted with honeycomb and mesh screens as flow straighteners. The test section is horizontal rectangular duct with cross-sectional area of 4cm height and 15cm width. Pressure taps are installed in the test section to measure the static pressure along the test section by using micro-manometer. In addition, pressure drop across orifice meter is measured by water U-tube manometer.

The tested heat sinks are located at 30cm from the test section entrance. All pin fin heat sinks are fabricated from aluminum 7050-T7350 (kAl=155 W/m.K) and have base dimensions of 15cm x 15cm x 2mm. Each pin fin has cross section area of cm x1 cm and its height is 2cm.

Ni- Chrome foil heater is used to provide electrical heating as uniform heat flux. Power consumption is determined by the voltage drop and current across the foil or by Wattmeter with accuracy of 1%. Thermal insulation is also used on the other surface of the heater assembly. The insulation system consists of a 3mm thick amiant layer (k = 0.35 W/m.K) followed by a 25mm thick glass wool layer (k = 0.041 W/m.K) and this is in turn followed by a 20mm thick wood board (k = 0.097 W/m.K).

In total, 12 copper–constantan (T type, 0.2mm) thermocouples are used. All the thermocouples are calibrated with the calibration device and the second-order standard mercury thermometer with an accuracy of 0.1 K. The fin array is instrumented with 7 thermocouples located on the middle and the root of fin along the flow direction. The other three are equipped on the insulation system, and other two on the inlet and outlet of the test section. The pressure drop is measured by pressure taps before and after heat sink.

B. Data Reduction

The thermal performance is measured at approach velocities of V= 2.4, 3.6, 4.8, and 7.2 m/s where Reynolds number range is from 10,000 to 25,000. In the experiments, it is assumed that the steady state conditions are achieved when the change in the base temperature of heat sink is less than 0.1oC in a time period about 3.5 hour. When these conditions are achieved, the base temperatures, the insulation system

temperatures, the power delivered to the heat sink, the approach velocity, the pressure drop across orifice meter, and pressure taps are recorded.

The approach velocity is estimated as:

$$V = C_d\sqrt{\frac{2g\Delta H}{\rho}} \quad (1)$$

where C_d is discharge flow coefficient, ΔH is pressure drop across orifice (manometer head) in mm h2o, ρ is air density in kg/m3, and g is gravitational acceleration in m/s2.

The temperature distribution along fin height can be neglected because of its small height so; the fin efficiency is not introduced. The total thermal resistance, Rth and the convective heat transfer rate, Qconv can be described as [7], [14]:

$$R_{th} = \frac{T_b - T_a}{Q_{conv}} = \frac{1}{hA_s} \quad (2)$$

where Tb is the mean base temperature of the heat sink, Ta is the ambient temperature, h is the convective heat transfer coefficient, As is the surface area of the heat sink, and Qconv is the convective heat transfer through the heat sink surfaces and is given by:

$$Q_{conv} = Q_{tot} - Q_{loss} = mC_p\left(T_{f,\text{out}} - T_{f,\text{in}}\right) \quad (3)$$

Qtot is the total amount of power supplied to heat sink, Cp is the specific heat capacity of air, m is the air mass flow rate through the test section. Qloss is the total amount of heat loss through insulation system and can be estimated as:

$$Q_{loss} = \frac{\Delta T}{\Sigma R_{ins}} \quad (4)$$

where ΔT is the temperature difference across the insulation system and ∑ Rins is the overall thermal resistance of the insulation system.

Reynolds number and Nusselt number based on the hydraulic diameter of test section are defined as:

$$Re_D = \frac{VD_h}{\upsilon} \quad (5)$$

$$Nu = \frac{hD_h}{k_f} = \frac{D_h}{R_{th}A_S k_f} \quad (6)$$

where Dh= 0.06315 m, kf is the air conductivity in W/m.K, and υ is air viscosity at inlet air temperature in m2/s. The friction factor (f) is calculated as:

$$f = \frac{2\Delta P}{\rho V^2 \frac{L}{D_h}} \quad (7)$$

where ΔP is the pressure drop across heat sink (Pa) and L is the distance between pressure taps (m).

C. Uncertainty Estimation

All instrumentations are independently calibrated. The uncertainty of the compound variables such as air density, thermal resistance, Reynolds number, Nusselt number, and friction factor can be calculated as follows [15], [16]:

Assume that Y is a given function of the independent variables x1, x2... xn. Thus Y=f (x1, x2…... xn) Let UY is the uncertainty in Y and Ux1, Ux2… Uxn are the uncertainties in the independent variables. The uncertainty in Y can be put in the differential form as:

$$U_Y^2 = \left[\left(\frac{\partial Y}{\partial x_1}U_{x_1}\right)^2 + \left(\frac{\partial Y}{\partial x_2}U_{x_2}\right)^2 + \left(\frac{\partial Y}{\partial x_3}U_{x_3}\right)^2 + \cdots + \left(\frac{\partial Y}{\partial x_n}U_{x_n}\right)^2\right] \quad (8)$$

The uncertainty of the compound variables can be estimated from this principle and the results of this analysis are summarized in Table I.

TABLE I
UNCERTAINTY OF COMPOUND VARIABLES

Compound Variable	Uncertainty (%)
Air Density	0.06
Thermal resistance	1.08
Reynolds number	1.25
Nusselt number	4.51
Friction factor	3.12

III. NUMERICAL ANALYSIS

The geometry of the theoretical model and the boundary conditions are illustrated in Fig. 2. The dimensions of the theoretical domain are 100cm × 4cm × 15cm (x×y×z). The thermal and flow fields are calculated numerically with commercial CFD software (Fluent 14). The system is assumed a steady state, incompressible, and turbulent flow. The fluid and the solid properties are constant, and the effects of gravitation and thermal radiation can be neglected. The equations governing the fluid state are the Reynolds-averaged Navier-Stokes equations and the energy equation. The general forms are expressed as:

$$\frac{\partial}{\partial x_i}(\rho V_i) = 0.0 \quad (9)$$

$$\frac{\partial}{\partial x_j}\left(\rho V_i V_j\right) = -\frac{\partial P}{\partial x_i} + \frac{\partial \tau_{ij}}{\partial x_j} \quad (10)$$

$$\frac{\partial}{\partial x_i}[V_i(\rho E + P)] = \frac{\partial}{\partial x_i}\left(k\frac{\partial T}{\partial x_i}\right) \quad (11)$$

where i is a tensor indicating 1, 2, 3 and τij is the viscous shear tensor.

In order to calculate the turbulent flow, standard k-ε turbulence model is selected and its equations is added to the governing equations and solved by CFD software.

$$\frac{\partial}{\partial x_i}(\rho V_i k) = \left(\mu + \frac{\mu_t}{\sigma_k}\right)\nabla^2 k + \mu_t S^2 - \rho\varepsilon \quad (12)$$

$$\frac{\partial}{\partial x_i}(\rho V_i \varepsilon) = \left(\mu + \frac{\mu_t}{\sigma_\varepsilon}\right)\nabla^2 \varepsilon + C_{\varepsilon 1}\frac{\varepsilon}{k}\mu_t S^2 - C_{\varepsilon 2}\rho\frac{\varepsilon^2}{k} \quad (13)$$

$$\mu_t = \frac{\rho C_\mu k^2}{\varepsilon} \quad (14)$$

The coefficients are (C_μ, σ_k, σ_ε, $C_{\varepsilon 1}$, $C_{\varepsilon 2}$) = (0.09, 1.0, 1.3, 1.44, 1.44) and $S = (S_{ij}S_{ij})^{0.5}$.

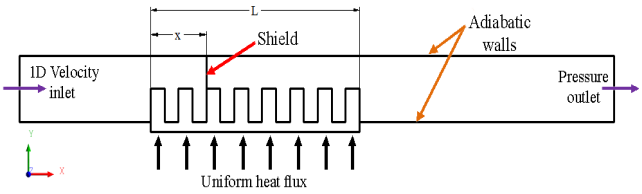

Fig. 2 Computational domain and boundary conditions

A. Mesh Sensitivity

Several unstructured grids are performed with different mesh sizes for heat sink without shield with approach velocity of 3.6 m/s in order to guarantee the grid independence of the results. The mesh is intensified between the fins to refine the numerical solution Fig. 3 shows the thermal resistance for 200,000, 400,000, 500,000, 800,000 and 1,000,000 grid sizes. According to this figure, the obtained results with 800,000 and 1,000,000 are very close where the maximum percentage error is about 0.3%. Therefore, the results from 1,000,000 grid size can be considered to be grid independence.

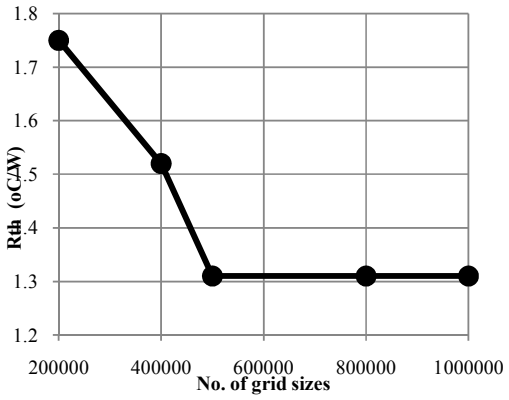

Fig. 3 Thermal resistance at different grid sizes

B. Code Validation

One case of heat sink without shield with approach velocity of 3.6 m/s and heating power of 40 W is selected to establish the validation process. A comparison between the predicted results by the numerical code and the present experimental data is performed in Fig. 4. This figure shows a good agreement between the predicted thermal resistance numerically and the present experimental measurements. Also, this numerical code is validated by comparing its predicted data with the experimental data measured by Zhang et al. [14] and obtains the same trend. Therefore, the present numerical code is valid to simulate the heat sinks.

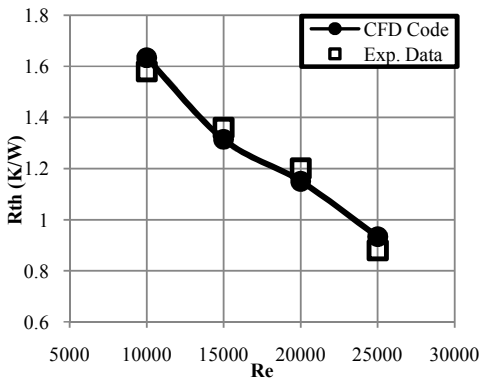

Fig. 4 Comparison between present experimental measurements and numerical code

IV. Results and Discussion

A. Thermal and Hydraulic Performance

After validation of the CFD code, either experimental or numerical data can be used to investigate the effect of Reynolds number and dimensionless shield position on the hydraulic and thermal performance of pin fin heat sink. Distribution of the velocity between fins is shown in Fig. 5. It is clear that, the maximum value of air velocity occurs under the shield where the smallest effective flow area at the shield cross-section.

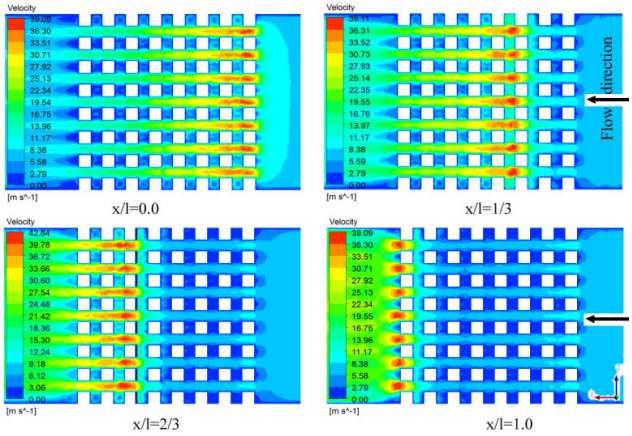

Fig. 5 Velocity distribution at y = 0.01 m at various shield positions for Re = 25000

Fig. 6 shows the temperature distribution over the floor of the heat sink at different shield position. It is found that, the lowest value of the temperature occurs at the shield where the maximum air velocity. The presence of the shield diminishes the temperature gradient over the base of heat sink. In the shield configuration, the lower temperature air is obstructed and forced into the inter-fin channel by the shield. The disturbance caused by air leaked into the inter-fin channel destroyed the boundary layer of fin. Meanwhile, the effective flow area at the shield cross-section decreased and the velocity in the inter-fin channel increased as shown in Fig. 5.

Therefore, the heat transfer performance of fin array is enhanced as the influence of shield as shown in Fig. 6.

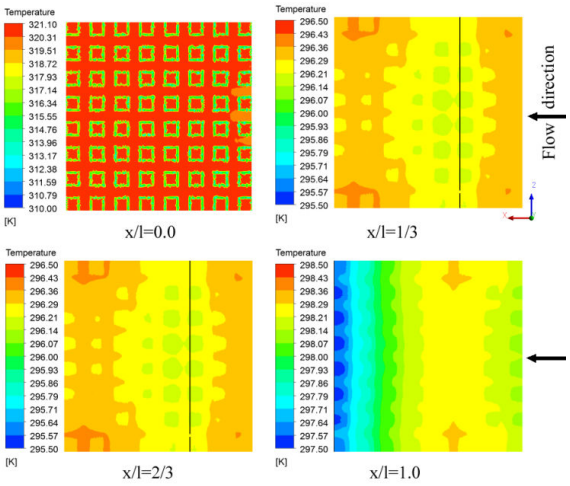

Fig. 6 Temperature distribution over heat sink base at various shield position for Re = 25000

The effect of Reynolds numbers on the thermal resistance is depicted in Fig. 7 for various position of the shield. The thermal resistance decreases as the Reynolds number increases and dimensionless shield position increases until x/l = 1/3 and then this behavior reverses. Therefore, the shield plays an important role in increasing the heat transfer around it.

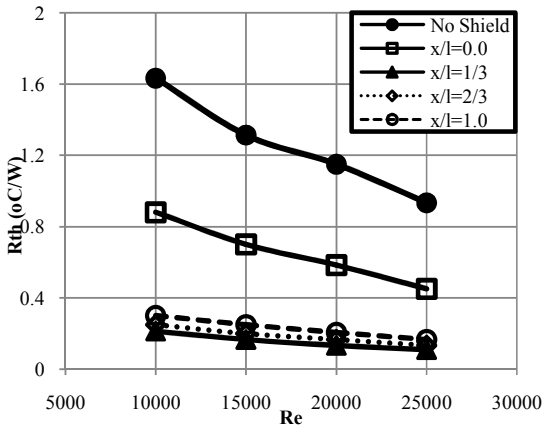

Fig. 7 Thermal resistance versus Reynolds numbers at different shield positions

The effects of Reynolds numbers on the Nusselt numbers are depicted in Fig. 8 for various shield position. The Nusselt number increases as the Reynolds number increases and dimensionless shield position increases until x/l = 1/3 and then this behavior reverses. The reason of such behavior is that the air before the shield at the entrance of the heat sink has low temperature and sinks and absorbs the heat from the heat sink. At the shield, the velocity increases and the heat transfer coefficient increases. As results, the region around the shield becomes cooler than any point on the base. Therefore, the impact of shield on the heat transfer performance is more significant at higher Reynolds number and the Nusselt number becomes the maximum value when dimensionless shield position is about 1/3.

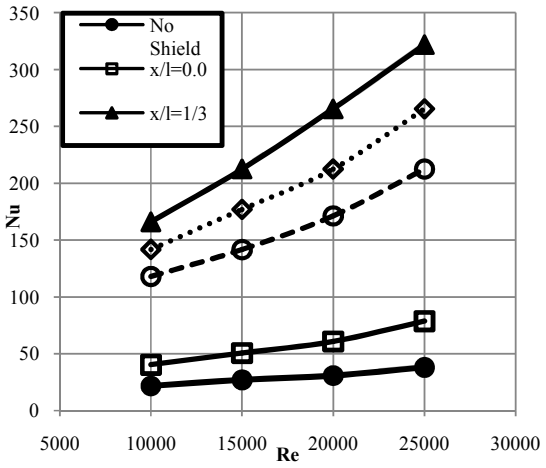

Fig. 8 Nusselt numbers versus Reynolds numbers at different shield positions

Fig. 9 depicts the effects of Reynolds numbers on the friction factors at various values of dimensionless shield position. The friction factor approximately decreases as the Reynolds number increases. As shown in Fig. 9, the friction factors increases due to the rise of the dimensionless shield position x/l. It is also found that the change of the friction factor is nearly same for x/l = 1/3 and 2/3 or x/l = 0.0 and 1.0. The maximum value of friction factor occurs at x/l = 1/3 and 2/3 where the shield at the middle region of the heat sink. The air in the inter-fin channel is gradually heated and leaked upward after the shield because of its lower density. Along the flow direction, the velocity of air increased gradually. Thus, the larger the dimensionless shield position is, the sharper the disturbance caused by shield is. Consequently, the flow resistance in the test section increased with the dimensionless shield position.

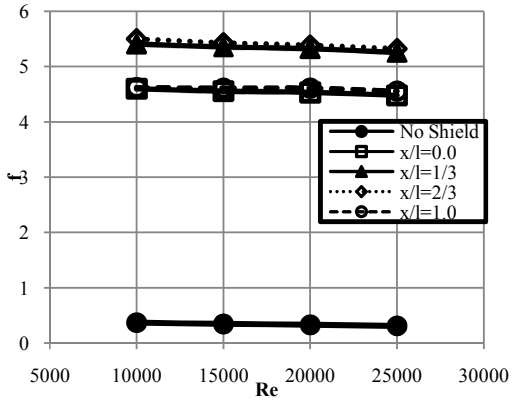

Fig. 9 Variation of friction factors with Reynolds numbers at different shield position

Fig. 10 illustrates the effect of dimensionless shield position on the thermal resistance at different Reynolds numbers. From this figure, it is found that, the thermal resistance decreases as the dimensionless shield position increases. This trend continues until x/l reaches to about 0.43. After this value, the thermal resistance increases as x/l increases. As results, the optimal value of dimensionless shield position is 0.43 from view point of thermal performance in the present study range of Reynolds numbers.

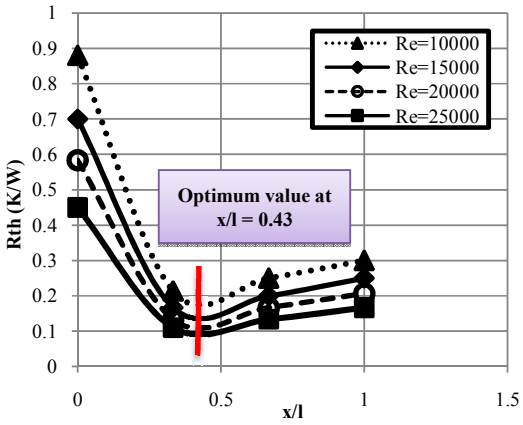

Fig. 10 Distribution of thermal resistance with shield position at different Reynolds numbers

B. Comprehensive Performance Evaluation of Shield Position

As mentioned above, all of these heat transfer promoters caused an increase of pressure loss. To comprehensively survey the influence of shield on the fin array performance, the evaluation approach based on identical pumping power criteria is adopted. The identical pumping power criterion is based on that the pressure drop is inversely proportional to the cubic of the air velocity, and measured by the value (Nu/Nu0)/(f/f0)1/3. When the value is greater than 1, it means that under the same pump power, the heat transfer rate of the enhanced heat transfer surface is larger than that of the reference surface.

Fig. 11 presents the comprehensive performance evaluation of fin array with different shield position, under identical pumping power criterion. It is noted that the ratio of (Nu/Nu0)/(f/f0)1/3 increased as the dimensionless shield position increased. In the present experimental range, the ratio is lower than 1 only when the shield position x/l = 0. Accordingly, the shield at the position x/l = 0 caused a decrease of fin array performance with the same pump power consumption. The fin array performance is improved as the shield installed in other positions. As the above discussion, the inlet section of fin array is not the optimum position for shield. And, the middle section at x/l = 0.43 is the optimum position of the shield as previously mentioned in Fig. 10.

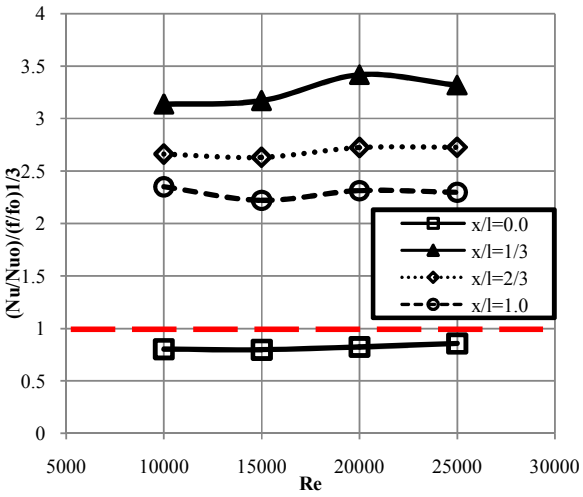

Fig. 11 Performance evaluations of fin array with different shield positions, under identical pumping power criterion

V. Conclusions

The effects of shield position without by-pass on the heat transfer and flow performances of fin array are experimentally and numerically investigated. These investigations have been reported and showed that CFD, an important tool in thermal engineering, is used to analyze the data generated by models representing the complexity of the flow patterns that evolve inter-fins. The standard k - ε turbulence model with enhanced wall treatment and viscous heating can be used to simulate this type of problems. This result is also considered in other paper [17].

The thermal resistance and the fiction factor decreases as the Reynolds number increases. The increase of the dimensionless shield position, the increase of Nusselt number until x/l reaches to 0.43. When x/l goes beyond this value, the Nusselt number decreases.

As the presence of the shield, the temperature gradient over the base of the heat sink is approximately diminished. The surface temperature distribution of the heat sink with shield at x/l = 1/3 or 2/3 is more uniform. This distribution is similar to the performance and behavior of the vapor chamber heat sink as mentioned in other papers [18], [19].

Under the identical pumping power criterion, the shield at the inlet section of fin array caused a decrease of fin array performance in present experimental and numerical range. The results show that the optimum shield position is at x/l = 0.43.

References

[1] R. W. Knight, J. S. Goodling, D. J. Hall, Optimal thermal design of forced convection heat sinks-analytical, ASMEJ. Electron. Packaging 113 (1991) 313-321.
[2] P. Teertstra, M. M. Yovanovich, J. R. Culham, T. Lemczyk, Analytical forced convection modeling of plate fin heat sinks, in: Proceedings of the Fifteenth IEEE SEMI-THERM Symposium, San Diego, CA, 1999, pp. 34-41.
[3] S. Lee, Optimum design and selection of heat sinks, in: Proceedings of the Eleventh IEEE SEMI-THERM Symposium, San Jose, CA, 1995, pp.48-54.

[4] M. A. Butterbaugh, S. S. Kang, Effects of airflow by-pass on the performance of heat sinks in electronics cooling, ASME Adv. Electron. Packaging 10 (2) (1995) 843-848.
[5] H. Shaukatullah, W. R. Storr, B. J. Hansen, M. A. Gaynes, Design and optimization of pin fin heat sinks for low velocity applications, in: Proceedings of the Twelfth IEEE SEMI-THERM Symposium, Austin, TX, 1996, pp.151-163.
[6] H. Jonsson, B. Moshfegh, Modeling of the thermal and hydraulic performance of plate fin, strip fin, and pin fin heat sinks-influence of flow by-pass, IEEE Trans. Components Packaging Technol.24 (2) (2001) 142-149.
[7] M. B. Dogruoz, M. Urdaneta, A. Ortega, Experiments and modeling of the hydraulic resistance and heat transfer of in-line square pin fin heat sinks with top by-pass flow, International Journal of Heat and Mass Transfer 48 (2005) 5058-5071.
[8] S. A. El-Sayed, S. M. Mohamed, A. M. Abdel-latif, A. E. Abouda, Investigation of turbulent heat transfer and fluid flow in longitudinal rectangular-fin arrays of different geometries and shrouded fin array, Experimental Thermal and Fluid Science 26 (2002) 879-900.
[9] H. Jonsson, B. Moshfegh, Enhancement of the cooling performance of circular pin fin heat sinks under flow by-pass conditions, in: Proceedings of the Eighth IEEE Inter Society Conference on Thermal Phenomena (ITHERM), San Diego, CA, 2002, pp.425-432.
[10] C. R. Biber, C. L. Belady, Pressure drop predictions for heat sinks: what is the best method? ASME Adv. Electron. Packaging 19 (2) (1997) 1829-1835.
[11] A. Dvinsky, A. Bar Cohen, M. Strelets, Thermo fluid analysis of staggered and in-line pin fin heat sinks, in: Proceedings of the Seventh IEEE Inter Society Conference on Thermal Phenomena (ITHERM), Las Vegas, NV, 2000, pp.157-164.
[12] H. Y. Li, G. L. Tsai, S. M. Chiang, J. Y. Lin, Effect of a shield on the hydraulic and thermal performance of a plate-fin heat sink, International Communications in Heat and Mass Transfer 36 (3) (2009) 233-240.
[13] G. Tsai, H. Y. Li, C. Lin, Effect of the angle of inclination of a plate shield on the thermal and hydraulic performance of a plate-fin heat sink, International Communications in Heat and Mass Transfer 37 (2010) 364-371.
[14] Y.-l. Zhang, J-p. Liu, D-t. Chong 2, J-j. Yan, Experimental investigation on the heat transfer and flow performances of the fin array with shield in bypass, International Journal of Heat and Mass Transfer 56 (2013) 674–682.
[15] R.J. Moffat, Contributions to the theory of single-sample uncertainty analysis, ASME Transactions Journal of Fluids Engineering 104 (1982) 250–258.
[16] R.J. Moffat, Describing the uncertainties in experimental results, Exp. Thermal Fluid Sci. 1 (1) (1988) 3–17.
[17] A. Al-Sarkhi, E. Abu-Nada, B.A. Akash, J.O. Jaber, Numerical investigation of shrouded fin array under combined free and forced convection, Int. Commun. Heat Mass Transfer 30 (3) (2003) 435- 444.
[18] H. Li, M. Chiang, C. Lee, W. Yang, Thermal performance of plate-fin vapor chamber heat sinks, International Communications in Heat and Mass Transfer 37 (2010) 731–738.
[19] H. Li, M. Chiang, Effects of shield on thermal-fluid performance of vapor chamber heat sink, International Journal of Heat and Mass Transfer 54 (2011) 1410-1419.